Multi-Frequency Synthetic Thinned Array Antenna for the Hurricane Imaging Radiometer

M. C. Bailey, *Life Senior Member, IEEE*, Ruba A. Amarin, *Member, IEEE*, James W. Johnson, *Senior Member, IEEE*, Paul Nelson, *Student Member, IEEE*, Mark W. James, David E. Simmons, Christopher S. Ruf, *Fellow, IEEE*, W. Linwood Jones, *Life Fellow, IEEE*, and Xun Gong, *Member, IEEE*

***Abstract*—A C-band four-frequency resonant stacked-patch array antenna is developed for synthetic thinned aperture radiometer measurements of hurricane force wind speeds. This antenna is being integrated into an aircraft instrument referred to as the Hurricane Imaging Radiometer (HIRAD). Details of the antenna design are presented along with antenna performance tests and laboratory measurements using a full-scale prototype array with a subset model of the HIRAD instrument.**

***Index Terms*—Microstrip antennas, multifrequency antennas, remote sensing, stacked microstrip antennas, synthetic aperture imaging.**

I. Introduction

THE airborne Hurricane Imaging Radiometer (HIRAD) is currently being developed by NASA's Marshall Space Flight Center in collaboration with NOAA and the Universities of Michigan and Central Florida. HIRAD will provide the accurate observations of ocean surface winds in the presence of intense rain that are required for forecast and warnings of tropical cyclones. NOAA's Stepped Frequency Microwave Radiometer (SFMR) is an aircraft borne remote sensor currently used for this purpose [1], and HIRAD will be an improvement on SFMR. The SFMR is nadir viewing and produces a surface wind profile along the ground track for each hurricane pass, whereas HIRAD will have a wide swath and, from an altitude of 20 km, image approximately 60 km of the storm on each pass. The HIRAD concept includes the multi-frequency C-band capability of the SFMR that has been performance proven and adds a form of electronic scanning with a stationary array antenna that is relatively new to earth remote sensing [2]. The result is the need for both multi-frequency, C-band operation and a scanning array radiometer system. HIRAD operates as an interferometer, sampling the spatial Fourier components of the cross-track brightness temperature scene.

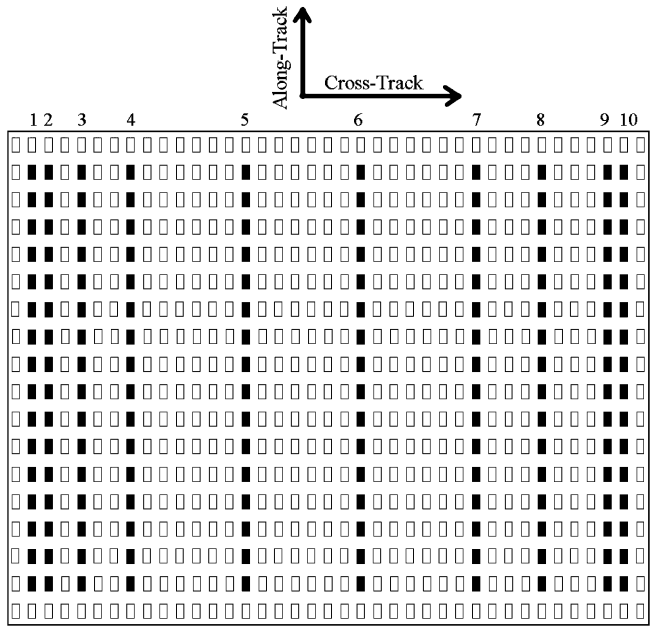


Fig. 1. Schematic of HIRAD array with active elements shown in black.

The HIRAD antenna is a microstrip array that operates simultaneously at four frequencies over approximately an octave bandwidth to enable the independent retrieval of wind and rain [3], [4]. The aircraft version of HIRAD currently being developed has a 0.82 m $\times$ 0.57 m array antenna with 37 $\times$ 16 individual 4-frequency elements as illustrated in Fig. 1. Each array element is a linearly polarized 4-frequency stacked-patch antenna oriented with the electric field vector polarized in the along-track direction. Additional terminated elements were placed around the periphery of the array in order to provide nearly the same array environment for all the elements for impedance matching purposes.

The array is thinned to 10 linear elements, shown as 10 lines of small solid rectangles in Fig. 1, each producing a fan beam pattern for cross-track synthesis and along-track pushbroom surface sampling. In the flight version, each linear element is fabricated with a 16-way uneven power combiner integrated onto the back of the array ground plane. These 10 elements, configured with 10 mutually coherent radiometers, taken in all possible pair combinations, can fully sample (at the Nyquist rate)

Manuscript received October 27, 2009; revised February 04, 2010; accepted February 05, 2010. Date of publication May 18, 2010; date of current version August 05, 2010. This work was supported by the HIRAD Project of the NASA Marshall Space Flight Center under a grant with the University of Alabama Huntsville Award NNM05AA22A.

M. C. Bailey is with the University of Central Florida, Orlando, FL and also with Applied EM, Hampton, VA 23666 USA (e-mail: m.c.bailey@cox.net).

R. A. Amarin, J. W. Johnson, P. Nelson, W. L. Jones, and X. Gong are with the University of Central Florida, Orlando, FL 32816 USA (e-mail: ramarin@mail.ucf.edu; jamesj@mail.ucf.edu; paulnelsonee@gmail.com; ljones@ucf.edu; xungong@mail.ucf.edu).

M. W. James is with NASA, Marshall Space Flight Center, Huntsville, AL 35806 USA (e-mail: Mark.W.James@nasa.gov).

D. E. Simmons is with the University of Alabama Huntsville, Huntsville, AL 35816 USA (e-mail: david.simmons@uah.edu).

C. S. Ruf is with the University of Michigan, Ann Arbor, MI 48109 USA (e-mail: cruf@umich.edu).

Digital Object Identifier 10.1109/TAP.2010.2050453

0018-926X/$26.00 © 2010 IEEE

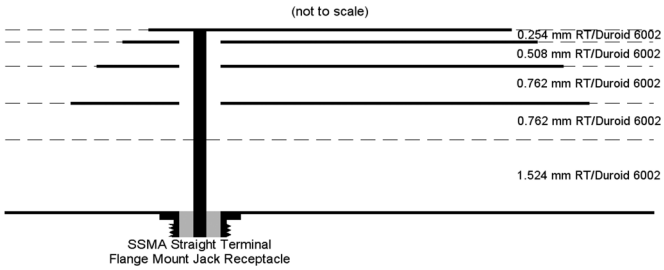


Fig. 2. Cross-sectional sketch of stacked-patch antenna (not drawn to scale).

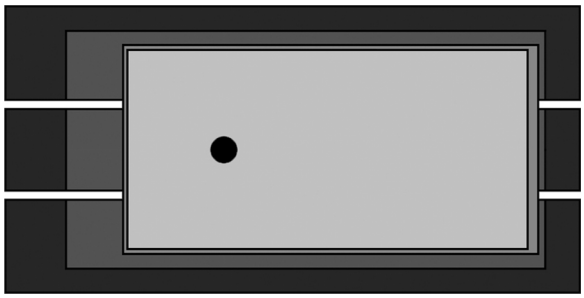


Fig. 3. Top view sketch of stacked-patch antenna.

all spatial components of the brightness temperature scene [5]. The HIRAD design produces a spatial resolution at nadir of 2.5 km at 4 GHz, from a 20 km altitude, and a field-of-view of approximately ± 60 degrees at all 4 frequencies, for a cross-track swath width of 60 km.

The individual array elements consist of 4 probe-fed, rectangular stacked patches, which in the original design resonated at 4, 5, 6, and 7 GHz. This wide frequency range required element spacing in the array to physically accommodate the lowest frequency radiators, but at the same time limit the spacing at the highest frequency to approximately 1/2 wavelength or less to limit grating lobe encroachment into the cross-track field-of-view. Given these constraints, the center-to-center spacing of individual elements was set at 38.1 mm along-track and 22.86 mm cross-track. It was later determined that an element pattern null could occur in the along-track direction near broadside with this array geometry; therefore, the upper frequency was reduced to 6.6 GHz in order to move this "array blindness" null out of the main beam of the along-track array factor.

Many papers are available in the literature describing the design of stacked-patch antennas of various configurations. These generally consist of dual-stacked or triple-stacked patches designed either for bandwidth enhancement or for multiple operating bands. In these stacked-patch concepts, the coupling between the patches of the stack becomes a significant consideration, requiring accurate computer modeling to achieve an acceptable design. Typically these designs are focussed on applications which require only a single antenna. In array applications, the coupling between stacked-patch elements of the array can also become a significant design consideration. This present effort extends the microstrip antenna technology to the design of quad-stacked patches in an array environment. Coupling between patches in the stack and also coupling between stacked-patch elements of the array are taken into consideration in the design process. Strategically located slots

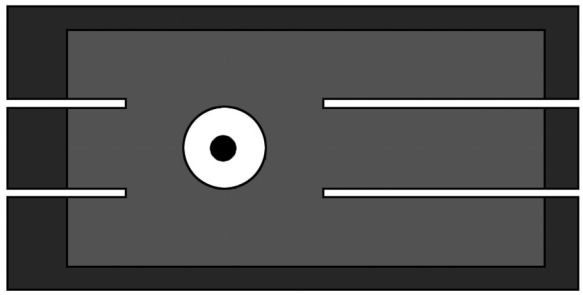


Fig. 4. Sketch of stacked-patch antenna with top two patches removed.

have been placed in the lower frequency patches to reduce cross-polarized radiation at the highest resonance.

This paper provides a detailed description of the individual element design and its evolution, with some emphasis on cross-polarization performance, plus full-scale prototype array test results and synthesized patterns from interferometer measurements. The prototype array design is currently being duplicated in a flight array for an aircraft flight instrument.

II. Element Design

The individual array elements for this present array development are four stacked-patches with a single probe feed soldered directly to the top patch and reactively coupled to the other three patches via a 2.794 mm diameter etched circle. Each patch is designed to resonate at a specific frequency while accounting for mutual coupling between stacked patches as well as coupling to adjacent stacked-patch elements of the array. The first design utilized square stacked-patches with equal thickness dielectric layers and included circular disks between patches to add capacitance for tuning out the inductance of the feed probe. Details of that earlier design are described in [6]. A commercially available method-of-moments (MoM) software package (ie3d) was used for all designs and another commercially available finite-element-method (FEM) software package (HFSS) was used later for further verification and analysis of the test results. Earlier comparisons between ie3d impedance simulations and laboratory measurements verified that the basic design was viable.

The present design differs from the earlier concept by: 1) removal of the embedded tuning disks due to fabrication difficulties; 2) change to rectangular patches with a 2:1 aspect ratio to reduce cross-pol and allow closer element array spacing cross-track; 3) use of narrow slots in the bottom two patches to further reduce cross-pol at the highest resonance; and 4) use of unequal dielectric thicknesses between patches to increase the bandwidth at the lower resonances. In order to avoid special ordered materials, standard commercially available substrate thicknesses, close to that desired, were used in the design. RT/Duroid 5880 was used as the substrate material in the earlier stages of development and the earlier laboratory proof of concept evaluations; however, RT/Duroid 6002 was selected for the final design and fabrication because of its superior thermal expansion properties. The present stacked-patch antenna concept is illustrated in Figs. 2–4 with the height of the cross-sectional view being exaggerated for visual clarity.

In the sketch of Fig. 4, the top two patches are removed to illustrate the etched slots in the bottom two patches. It

TABLE I
DIMENSIONS OF STACKED-PATCH ANTENNA ELEMENTS

	Patch #1 (bottom)	Patch #2	Patch #3	Patch #4 (top)
Resonant Frequency (GHz)	4.0	5.0	6.0	6.6
Dielectric Thickness (mm)	2.286	0.762	0.508	0.254
Patch Length (mm)	19.406	16.180	13.945	13.538
Patch Width (mm)	9.7028	8.0772	7.0104	6.7564
Feed offset wrt patch center (mm)	2.3114	2.7559	3.5941	3.4925
Diameter of feed probe (mm)	0.8636	0.8636	0.8636	0.8536
Diameter of etched circle (mm)	2.794	2.794	2.794	n/a
Separation of slots (mm)	2.794	2.794	n/a	n/a
Width of slots (mm)	0.254	0.254	n/a	n/a
Length of slots (mm)	4.0132 8.6360	1.9558 7.4676	n/a n/a	n/a n/a

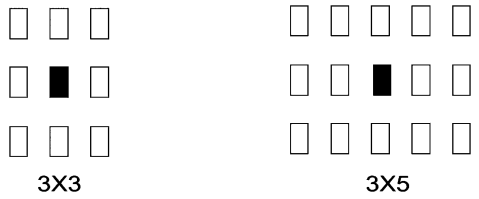


Fig. 5. Partial array configurations for computer simulations of embedded element impedance (3 × 3 cluster) and patterns (3 × 5 cluster).

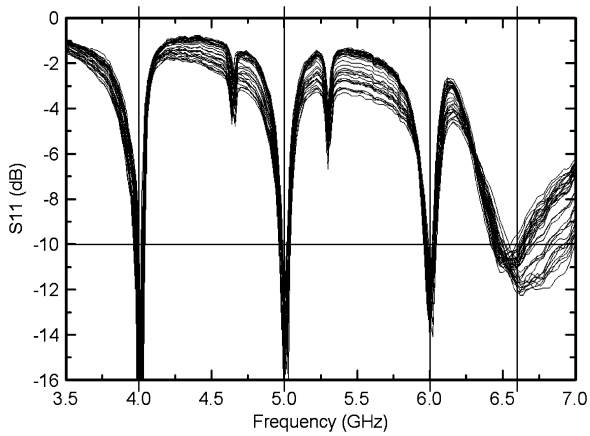


Fig. 6. Measured reflection coefficients for one panel (40 active elements) of the prototype array.

was observed during computer simulations that, when the stacked-patch antenna is placed in the array environment, significant cross-polarized radiation was observed at the highest resonance, due to mutual coupling with cross-polarized currents excited on the bottom patches of the adjacent elements. These slots were etched on the bottom patches to disrupt those orthogonal currents in an attempt to encourage the current to flow more in the desired direction. Computer model simulations indicated that indeed a reduction of cross-polarized radiation at the highest resonance could be realized; therefore, all the stacked-patch elements in the final array were fabricated with these slots. Dimensions for the final antenna element design are listed in Table I.

Because of the large computer memory and CPU time required for accurate modeling of the array, a partial array of elements was used to design the stacked-patch antenna element. This partial array allows mutual coupling between adjacent stacked-patch elements to be included in the impedance matching for the embedded element. The 9 × 9 impedance and scattering matrices were used to analyze the impedance characteristics of the central element of a 3 × 3 cluster. The stacked-patch element embedded radiation patterns were modeled in a similar manner using a 3 × 5 cluster. These partial arrays are illustrated in Fig. 5.

A full-size laboratory prototype array was fabricated with SSMA connectors on all of the active elements and resistive chip terminations on the inactive elements. This array served as a test article to evaluate the design. The SSMA connectors allowed for testing each individual stacked-patch element of the 160 active array elements. The prototype array was fabricated as four panels each consisting of 40 active elements. These four panels were joined on a common ground plane to form the complete array. The swept frequency measurement of the input reflection coefficient for each stacked-patch element on one panel of the array is shown in Fig. 6. The data in Fig. 6 are representative of measurements on the other three panels. The data in Fig. 6 shows some small variations between individual elements, which could be attributed to hand installation and soldering of SSMA connector probes.

Fig. 7 shows reflection coefficient measurements on two elements located on lines 1 and 5 of the array compared with predicted results. The short dashed curve in Fig. 7 was calculated for the center element in a 3 × 3 cluster with dielectric layers of infinite extent. The measured resonant frequencies agree with the design predictions and, although the measurements did not exhibit the predicted deep resonances at the higher frequencies, the impedance match was considered sufficient to proceed with development of a flight model of the HIRAD instrument using this antenna design.

To further examine the differences between the results, another commercially available software package (HFSS) using the finite element method was used to model the element. The results of this model for the center element of the 3 × 3 cluster are compared in Fig. 8 with the measured data. This model tends to predict the depth of the higher frequency resonances more

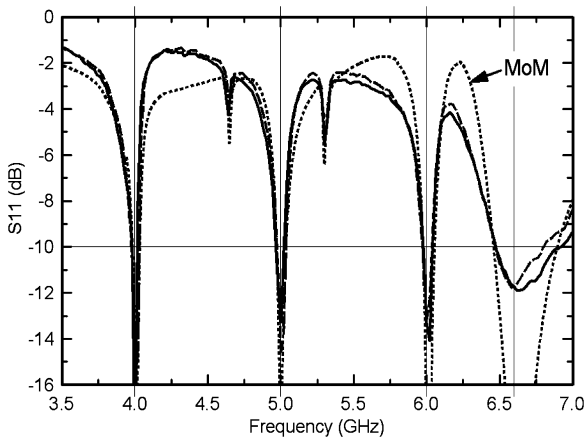


Fig. 7. Reflection coefficient for two elements of the prototype array (solid = line 5) (long dash = line 1) (short dash = calc. for 3 × 3 array center element).

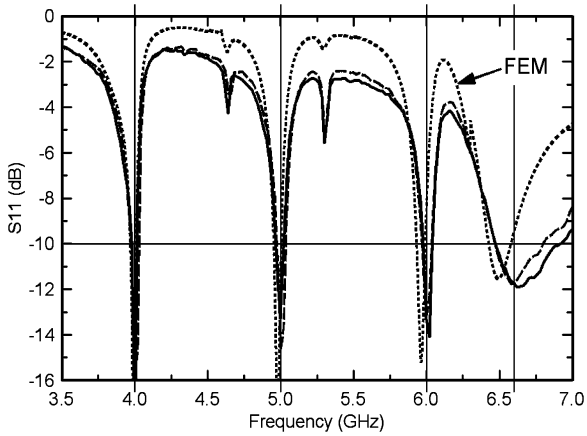


Fig. 8. Reflection coefficient for two elements of the prototype array (solid = line 5) (long dash = line 1) (dash = calc. for 3×3 array center element).

accurately and provide additional verification of the laboratory measurements.

The two smaller dips in the S11 curves on either side of the 5 GHz resonance in Fig. 7 and Fig. 8 are attributed to the slots in the bottom patches, which were described earlier. These artifacts were not observed on previous array test articles and simulations without the slots.

The effect of the slots on cross-pol patterns is illustrated by comparing the calculated element patterns with and without the slots in Fig. 9 for a single element (1 × 1) and in Fig. 10 for the central element in a 3 × 5 cluster (3 elements in the E-plane direction and 5 elements in the H-plane direction). These patterns were obtained from the MoM model, which used the planar dielectric Green's function. These results demonstrate that the slots had no effect on the cross-pol pattern for the single isolated element; however, the slots did reduce the maximum cross-pol level by about 8 dB in the 3 × 5 cluster where the active element is surrounded by other elements and mutual coupling to cross-polarized currents on adjacent patches becomes significant. Rippling in the patterns of Fig. 10 are attributed to the

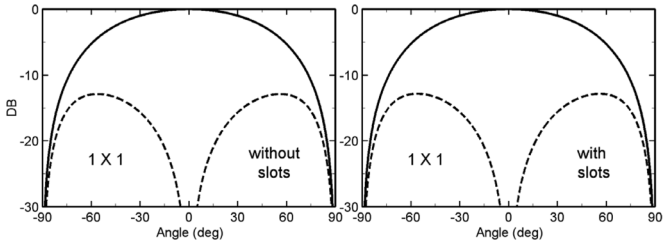


Fig. 9. Cross-track (H-plane) element patterns at 6.6 GHz for single isolated element (co-pol solid) (cross-pol dashed).

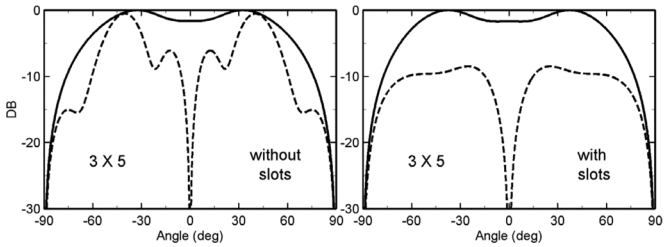


Fig. 10. Cross-Track (H-plane) element patterns at 6.6 GHz for the central element of 3 × 5 cluster (co-pol solid) (cross-pol dashed).

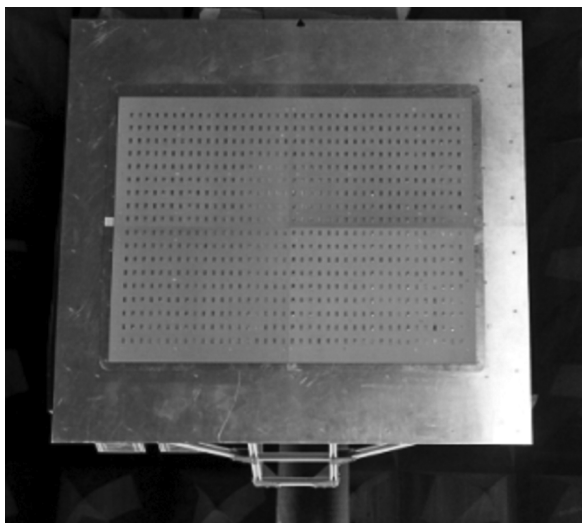


Fig. 11. HIRAD prototype with the array mounted on a large ground plane.

small finite size (5 elements) of the array in the pattern direction. A larger array could not be modeled with sufficient accuracy due to the large number of unknowns required in the numerical model simulation.

III. Array Tests and Characterization

A full-scale prototype array was fabricated and fully characterized in the Marshall Space Flight Center anechoic chamber as shown in Fig. 11. The prototype antenna is a complete 37 × 16 array, with a line of matching elements around the perimeter and the array was thinned to 10 linear elements as illustrated in Fig. 1. A 16-way connectorized power combiner was attached to each of the 10 linear elements. Two radiometers were mounted in a supporting structure behind the array and translated along the back of the array to mate with the 10 power combiners.

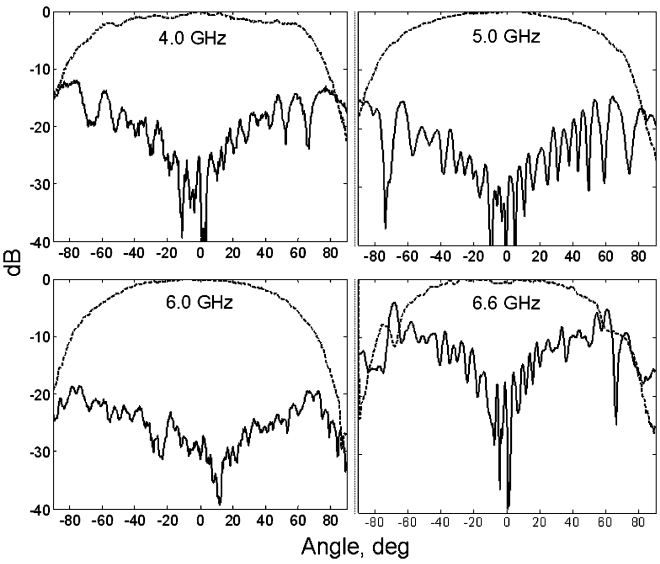


Fig. 12. Measured cross-track patterns for linear element # 5 (co-pol dashed) (cross-pol solid).

Two sets of measurements were made, individual patterns in the 2 principal planes to characterize the 10 linear elements, and interference patterns for all combinations (i.e., pairs) of the linear elements to characterize the system as an interferometer. The pair of coherent radiometers was used in measuring the interferometer interference patterns. Each radiometer provided a power measurement for each of the linear elements, and all pairs of radiometers provided a complex multiplication of 2 respective signals for the interference patterns. The interference patterns are the impulse response of the array for each linear element pair in the interferometer, and define the spatial filtering. Synthesized array patterns over the HIRAD swath, which also characterize the array, may be computed from the interference patterns. The conventional range measurement, with a coherent source and square-law detector, was used for element pattern measurements to provide the large dynamic range required, particularly for the along-track patterns.

A. Element Patterns

Fig. 12 shows co-pol and cross-pol patterns at each of the four frequencies for linear element #5 near the center of the array. One would notice that the cross-pol level for the measured patterns at 6.6 GHz is very close to that calculated in Fig. 10 for the 3×5 cluster. This demonstrates that the cross-pol reducing slots are working as expected.

The measured cross-track pattern for linear element #5 at 6.6 GHz is compared in more detail in Fig. 13 with the MoM and FEM model calculations for the center element of a 3×5 cluster. Due to the much larger computer memory required, a larger array could not be accurately modeled; however, the 3×5 array model should provide sufficient interelement mutual coupling effects upon radiation patterns for elements near the center of the array. The MoM model is for dielectric layers of

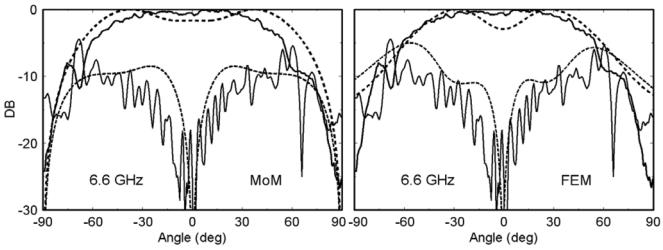


Fig. 13. Comparison of cross-track patterns at 6.6 GHz (solid = measured)(dash = calculated 3×5 cluster).

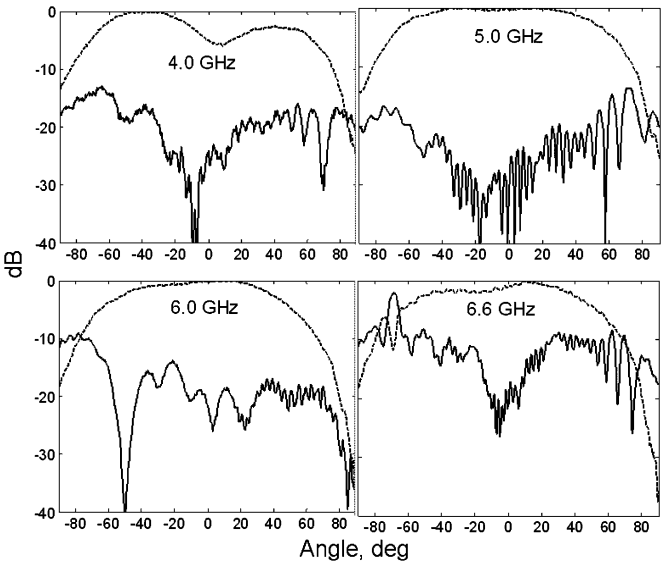


Fig. 14. Measured cross-track patterns for linear element #1 (co-pol dashed) (cross-pol solid).

infinite extent; whereas, the FEM model is for truncated dielectric layers; thus causing a difference in the pattern ripple due to the finite array and finite structure. The test article was a much larger array, which results in a higher spatial frequency ripple in the measured patterns. Although there is some difference in the shape of the patterns for the two simulation models, the measured cross-pol level is very close to the predictions for both models.

The co-pol and cross-pol patterns at each of the four frequencies for linear element #1 at the edge of the array are shown in Fig. 14. Patterns for linear elements in the central part of the array tend to be essentially the same as that for linear element #5, whereas the patterns for linear elements at the edge of the array tend to show an asymmetry, e.g. the cross-track patterns for #10 are the mirror images of the patterns for #1. This asymmetry in the cross-track patterns for elements near the edge of the array is characteristic of the asymmetry expected for arrays with inter-element mutual coupling. Mutual coupling for this stacked-patch array is much stronger at 4.0 GHz than for the other resonances; therefore, the asymmetric distortion in the 4.0 GHz co-pol pattern in Fig. 14 tends to be more pronounced.

The along-track patterns for all 10 linear elements were essentially the same as #5, which is shown in Fig. 15. The power

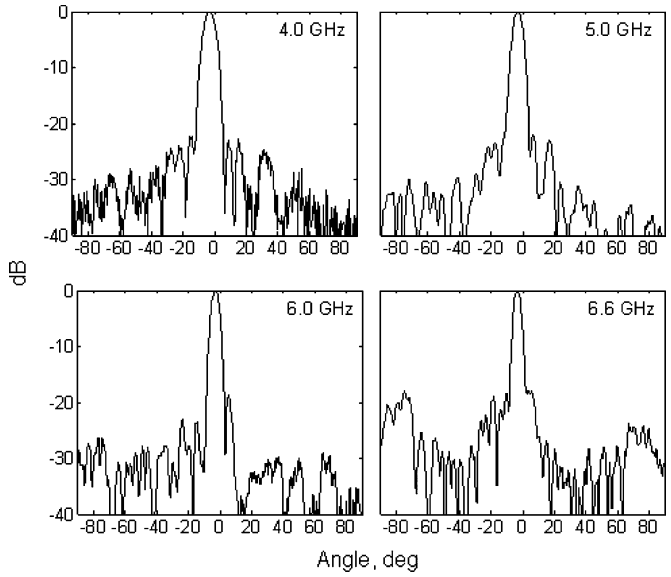


Fig. 15. Measured along-track Co-Pol patterns for linear element 5.

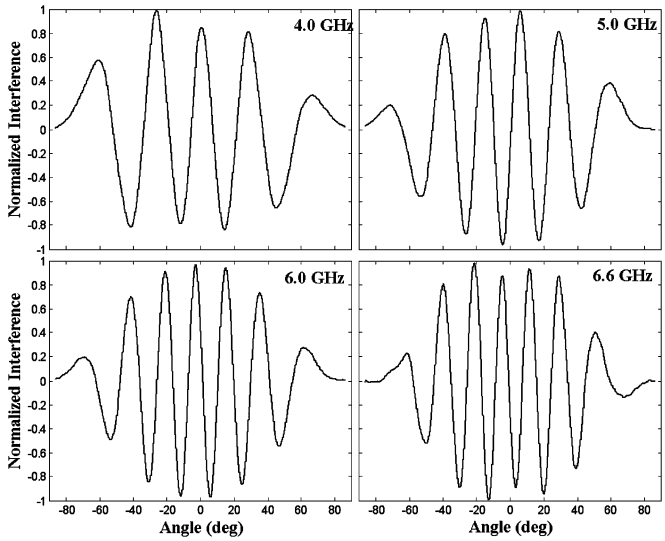


Fig. 16. Measured interference patterns for baseline $n = 7$ (linear elements #5 and #6).

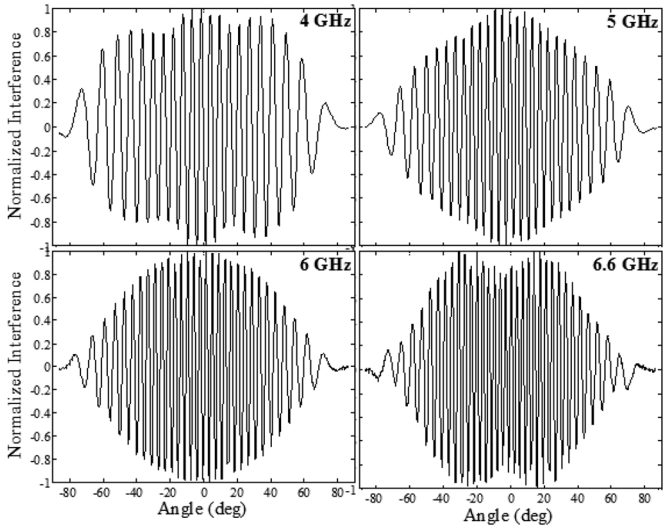


Fig. 17. Measured interference patterns for baseline n $= 34$ (linear elements #2 and #9).

combiners contained a tapered amplitude distribution to lower the along-track sidelobes.

B. Array Patterns

For a 1-D interferometer imager such as HIRAD, the complex output products (visibilities) for all element pairs in the thinned array are a function of the cross-track scene brightness temperature, $T_b(\theta, \phi)$, the element patterns, and the interference patterns. In general, the Fourier decomposition of the brightness temperature scene by the interferometric measurement is described by [2]

$$V(v) = \int_{-\pi/2}^{\pi/2} \int_{0}^{\pi} T_b(\theta,\phi) F(\theta,\phi) e^{j2\pi(-v \sin\theta \sin\phi)} \sin\theta \quad d\theta d\phi \tag{1}$$

where $V(v)$ is the visibility for each interferometer baseline (element pair spacing), v is the spacing in wavelengths, $F(\theta, \phi)$ is the product of the 2 element voltage patterns at each baseline, and the exponential term is the interference pattern for each baseline.

Equation (1) can be simplified for the one-dimensional case by eliminating the variable θ and using a matrix formulation, as given by

$$\underset{(N\times 1)}{V} = \underset{(N\times P)}{G} \times \underset{(P\times 1)}{T_b} \tag{2}$$

where N is the total number of visibilities, or baselines, and P is the number of pixels in the brightness temperature scene. The matrix 'G' is populated with the complete set of measured interference patterns and fully characterizes the spatial frequency response of the array. In practice, a brightness temperature image is formed from the measured visibility by operating the pseudo-inverse of G on V to estimate T_b. A pseudo-inverse, such as the Moore-Penrose version, is used because N and P are typically not equal.

The conditioning of G is generally not an issue during the inversion process. The matrix, viewed as a linear operator, is to first order a Discrete Fourier Transform (DFT) of the image vector, T_b. Second order effects, such as inter-element mutual coupling, introduce small deviations from an ideal DFT. This requires the operator to be inverted using a least squares pseudo-inverse method as opposed to an analytical inverse DFT. However, the conditioning of G is dominated by its DFT component, which is well suited to inversion. In practice, the inversion is found to be very stable provided all necessary Fourier components of the brightness temperature are sampled, up to the maximum component determined by the physical dimensions of the synthesized array (which they are).

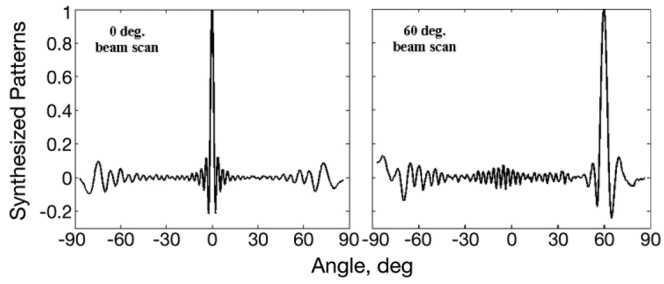


Fig. 18. Synthesized patterns from radiometer measurements at 6.6 GHz.

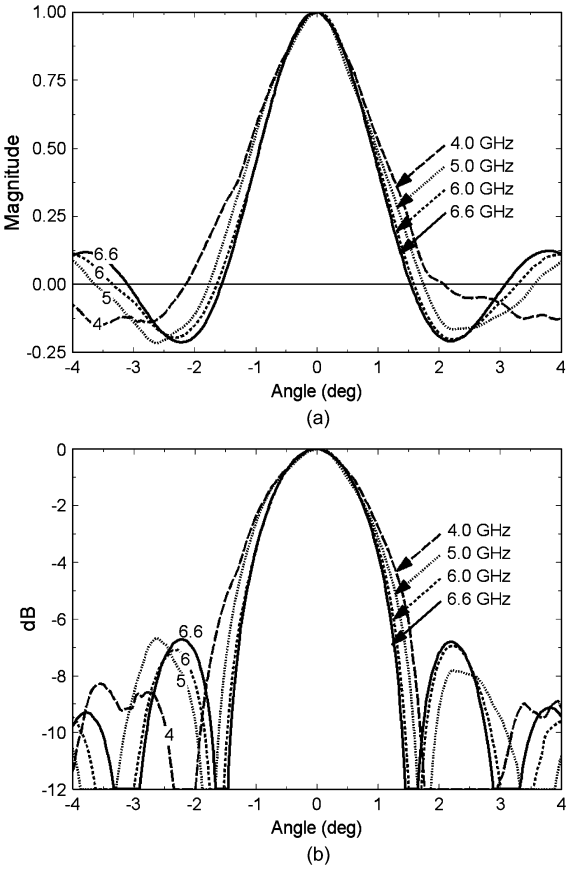


Fig. 19. Synthesized patterns from radiometer measurements at all four frequencies for zero beam scan (a) linear scale (b) log scale.

Since T_b was a point source in the chamber tests, (1) shows that for each scan, the measured visibility (interference pattern) is a sinusoid at a spatial frequency determined by the baseline, $v = nd/\lambda$, with an envelope equal to the product of the two element voltage patterns. For the HIRAD design, $n = 1$–36 and d is the minimum spacing between linear elements. The maximum spacing is $36d$; therefore, the spatial frequencies of the visibilities measured in the chamber will vary from < 1 Hz to 36 Hz over the 4.0 to 6.6 GHz operating frequency range.

Both co-pol and cross-pol interference patterns were measured for each of the 36 baselines, fully populating a G-matrix at each of the 4 frequencies. The patterns at all four frequencies for baselines 7 and 34 are shown in Figs. 16 and 17 as examples. Interior array elements #5 and #6 were used to form the interference patterns in Fig. 16 for baseline $n = 7$ and the envelope ripple is relatively small compared to that in Fig. 17, where the outside elements #2 and #9 were used. The envelope ripple in the 4 GHz and 6.6 GHz patterns is due to the ripple in the element patterns.

Synthesized array patterns were computed from the measured G-Matrix using the method described by LeVine [7], which is based on the inversion of (2). A full 180° pattern with boresight angle at any pixel in the T_b scene can be computed once the array is characterized by the G-matrix. Fig. 18 includes two examples showing synthesized patterns at 0° and 60° scan angles for 6.6 GHz. These demonstrate the negative sidelobes that are characteristic of complex correlation radiometers.

Fig. 19 shows synthesized patterns at all four frequencies on both linear and log scales, expanded about the zero scan angle to emphasize the main beam and near-in sidelobes. The 6.6 GHz beamwidth is the narrowest at approximately 1.8°, which is expected for an array of this size, and the beamwidth varies properly in accordance with the other frequencies. Main beam half-power widths for synthesized patterns of interferometer arrays are typically 1/2 the beamwidth for real (filled) apertures of the same size [2]. The first sidelobes were symmetric about the main beam in the 0° case and at a level of approximately −6.7 dB, which is expected for a uniform array taper with synthesized patterns, as compared to −13.3 dB sidelobes for a real aperture.

IV. Conclusions

A four-frequency synthetic thinned array of stacked-patch elements was designed, fabricated and prototype tested for the Hurricane Imaging Radiometer. Based upon this successful laboratory evaluation, an aircraft flight qualified model of this antenna is being integrated with the HIRAD instrument for mapping of severe oceanic storms.

References

[1] E. W. Uhlhorn, P. G. Black, J. L. Franklin, M. Goodberlet, J. Carswell, and A. S. Goldstein, "Hurricane surface wind measurements from an operational stepped frequency microwave radiometer," *Monthly Weather Rev.*, vol. 135, no. 9, pp. 3070–3085, 2007.

[2] A. B. Tanner and C. T. Swift, "Calibration of a synthetic aperture radiometer," *IEEE Trans. Geosci. Remote Sensing*, vol. 31, pp. 257–267, Jan. 1993.

[3] J. Johnson, R. Amarin, S. El-Nimri, L. Jones, and M. Bailey, "A wide-swath, hurricane imaging radiometer for airborne operational measurements," presented at the IGARSS, Denver, CO, 31 July–4 Aug. 2006.

[4] C. Ruf, R. Amarin, M. C. Bailey, B. Lim, R. Hood, M. James, J. Johnson, L. Jones, V. Rohwedder, and K. Stephens, "The hurricane imaging radiometer—An octave bandwidth synthetic thinned array radiometer," presented at the IGARSS, Barcelona, Spain, Jul. 23–28, 2007.

[5] C. S. Ruf, "Numerical annealing of low redundancy linear arrays," *IEEE Trans. Antennas Propag.*, vol. 41, no. 1, pp. 85–90, 1993.

[6] M. C. Bailey, Stacked-patch antenna element design for multi-frequency array applications Research Triangle Institute Tech. Rep. RTI/8348/026-01F, Sep. 2005, NASA Contract NAS1-02057, Task Order No. 7026.

[7] D. M. Le Vine, A. J. Griffis, C. T. Swift, and T. J. Jackson, "ESTAR: A synthetic aperture microwave radiometer for remote sensing applications," *Proc. IEEE*, vol. 82, no. 12, Dec. 1994.



M. C. Bailey (S'69–M'71–SM'81–LSM'02) received the B.S. degree in electrical engineering from Mississippi State University, Starkville, in 1964, the M.S. degree in electrical engineering from University of Virginia, Charlottesville, in 1967, and the Ph.D. degree in electrical engineering from Virginia Polytechnic Institute and State University, Blacksburg, in 1973.

He is currently employed part-time by Applied EM, Hampton, VA and also serves as a Technical Consultant for the University of Central Florida, Orlando. He previously worked for Research Triangle Institute, Hampton, VA after retiring from NASA, Langley Research Center, Hampton, VA in 2000 with 36 years of federal government employment as a research engineer. He was a Visiting Professor at the University of Mississippi, Oxford, during the 1978–79 academic year. He has authored or coauthored over 110 publications in the field of antennas and electromagnetics. He coauthored the section "Antennas and Wave Propagation" in the *Electronics Engineers' Handbook* (McGraw-Hill, 1982, 2nd ed), and coauthored the chapter "Radiometer Antennas" in the *Antenna Engineering Handbook* (McGraw-Hill, 1984, 2nd ed).

Dr. Bailey has been the recipient of 27 NASA awards for recognition of technical accomplishments, including the NASA Medal for Exceptional Scientific Achievement.



Ruba A. Amarin (M'06) received the B.A. degree in electronic engineering from the Princess Sumaya University for Technology, Amman-Jordan, in 2004 and the M.S. degree in electrical engineering from the University of Central Florida, Orlando, in 2006. She is currently working toward the Ph.D. degree at the University of Central Florida, Orlando, under the supervision of Dr. Linwood Jones.

She is conducting research in satellite remote sensing at the University of Central Florida.



James W. Johnson (SM'81) is a native of Virginia. He received the B.S. and M.S. degrees in electrical engineering from Virginia Polytechnic Institute, Blacksburg, in 1966 and 1969, respectively.

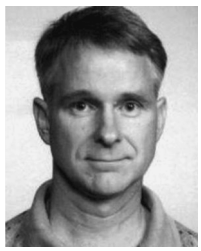
He began a career at the NASA, Langley Research Center in Hampton, VA, in 1966 and retired in 2006. He is currently a Visiting Research Scientist with the Central Florida Remote Sensing Lab, University of Central Florida, Orlando. During his time with NASA his primary concentration was in microwave remote sensing for earth sciences. He developed techniques for measuring ocean surface and polar ice characteristics using active and passive microwave systems. This included the development of multi-frequency techniques to measure the height statistics and spectral characteristics of ocean surface waves. He served as the NASA project engineer for the development of the SeaSat Wind Field Scatterometer, which was launched in 1978. He later led conceptual design studies and technology development projects for various earth science applications, with a brief interruption for program and project management positions in the Space Station Program at NASA Headquarters and at Langley.



Paul Nelson (S'08) received the B.S. degree in electrical engineering from the University of Central Florida, Orlando (UCF), in 2008, where he is currently working toward the M.S. degree.

Since, 2007, he has engaged research at the Antennas, RF and Microwave Integrated systems (ARMI) Laboratory at UCF, as an undergraduate and graduate student. His research interests include stacked-patch microstrip antenna array design and time difference of arrival direction finding systems.

Mr. Nelson is a recipient of the undergraduate IEEE MTT-S Scholarship Award in 2007, as well as the Science, Mathematics, and Research for Transformation (SMART) Scholarship in 2008.



Mark W. James received the B.S. degree in electrical engineering technology from Purdue University, West Lafayette, IN, in 1978 and the B.S. degree in electrical and computer engineering from the University of Michigan, Ann Arbor, in 1984.

He is currently employed by NASA, Marshall Space Flight Center, Huntsville, AL, in the Engineering Directorate. He has worked previously at the Space Physics Research Laboratory, University of Michigan, Daedalus Enterprises, and Delco Electronics. He has coauthored in the areas of microwave and near-infrared remote sensing. He has been involved in the development of microwave radiometers, Near IR and visible spectrum airborne spectrometers, data acquisition systems and lightning detection sensors.

Mr. James is a registered Professional Engineer in the State of Alabama. He has received numerous NASA awards including the Directors Commendation for technical excellence and Exceptional Service Award.



David E. Simmons received the B.S. degree in electrical engineering from Tennessee Technological University, Cookeville, in 1979.

He is currently employed by the University of Alabama, Huntsville. He has previously worked for BAE Systems/MEVATEC, Jacobs/Sverdrup, Chrysler, GTE and Honeywell. He has served in various technical roles since graduation on commercial, DoD and NASA projects. He has designed and supported airborne passive radiometer system electronics, missile testing, flight experiments, automotive and telephony electronics testing and military communications equipment.



Christopher S. Ruf (S'85–M'87–SM'92–F'01) received the B.A. degree in physics from Reed College, Portland, OR, and the Ph.D. degree in electrical and computer engineering from the University of Massachusetts, Amherst.

He is currently a Professor of atmospheric, oceanic, and space sciences and electrical engineering and computer science and Director of the Space Physics Research Laboratory, University of Michigan, Ann Arbor. He has worked previously at Intel Corporation, Hughes Space and Communication, the NASA Jet Propulsion Laboratory, and Penn State University. In 2000, he was a Guest Professor with the Technical University of Denmark, Lyngby. He has published in the areas of microwave radiometer satellite calibration, sensor and technology development, and atmospheric, oceanic, land surface and cryosphere geophysical retrieval algorithms.

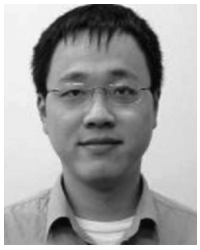
Dr. Ruf is a member of the American Geophysical Union (AGU), the American Meteorological Society (AMS), and Commission F of the Union Radio Scientifique Internationale. He has served on the Editorial Boards of the AGU *Radio Science*, the IEEE TRANSACTIONS ON GEOSCIENCE AND REMOTE SENSING (TGRS), and the AMS *Journal of Atmospheric and Oceanic Technology*. He is currently the Editor-in-Chief of the IEEE TRANSACTIONS ON GEOSCIENCE AND REMOTE SENSING. He has been the recipient of three NASA Certificates of Recognition and four NASA Group Achievement Awards, as well as the 1997 TGRS Prize Paper Award, the 1999 IEEE Resnik Technical Field Award, and the IGARSS 2006 Symposium Prize Paper Award.



W. Linwood Jones (SM'75–F'99–LF'09) received the B.S. degree in electrical engineering from the Virginia Polytechnic Institute, Blacksburg, in 1962, M.S. degree in electrical engineering from the University of Virginia, Charlottesville, in 1965, and the Ph.D. degree in electrical engineering from the Virginia Polytechnic Institute and State University, Blacksburg, in 1971.

He is currently a Professor with the School of Electrical Engineering and Computer Science at the University of Central Florida in Orlando. At UCF, he teaches undergraduate and graduate courses in communications, satellite remote sensing and radar systems. Also, he is the director of the Central Florida Remote Sensing Laboratory where he performs research in satellite microwave remote sensing technology development. Prior to becoming a college professor in 1994, he had 27 years federal government employment with NASA at the Langley Research Center in Hampton, VA; at NASA Headquarters in Wash DC and at the Kennedy Space Center, FL. Further, he spent eight years in the private aerospace industry with employment at General Electric's Space Division in King of Prussia, PA and Harris Corp.'s Government Aerospace Systems Division in Melbourne, FL.

Prof. Jones is a member of the American Geophysical Union (AGU) and Commission F of the Union Radio Scientifique Internationale. For education, he received the IEEE Orlando Section: Outstanding Engineering Educator Award 2003, the College of Engineering: Excellence in Undergraduate Teaching Award 2004, and the IEEE Florida Council: Outstanding Engineering Educator Award 2004. For his research, he received four NASA Special Achievement Awards, seven NASA Group Achievement Awards, the CNES Space Medal, the Aviation Week & Space Technology Space Program Award -1993, and the Naval Research Lab 2004 Alan Berman Research Publications Award.



Xun Gong (S'02–M'05) received the B.S. and M.S. degrees in electrical engineering from FuDan University, Shanghai, China, in 1997 and 2000, respectively, and the Ph.D. degree in electrical engineering from the University of Michigan, Ann Arbor, in 2004.

He is currently an Assistant Professor of electrical engineering and computer science at University of Central Florida, Orlando. He was with the Birck Nanotechnology Center at Purdue University, West Lafayette, IN, as a Postdoctoral Research Associate in 2005. His research interests include high-Q resonators and filters, microwave sensors, integrated RF front-end, flexible electronics, and packaging.

Dr. Gong is a member of the IEEE Microwave Theory and Techniques Society (IEEE MTT-S), the IEEE Antennas and Propagation society (IEEE AP-S), and the International Microelectronics and Packaging Society (IMAPS). He is the recipient of the NSF Faculty Early CAREER Award in 2009. He is the recipient of the Third Place Award in the Student Paper Competition presented at the 2004 IEEE MTT-S International Microwave Symposium (IMS), Fort Worth, TX.